BIOPHYSICS

Hidden vibronic and excitonic structure and vibronic coherence transfer in the bacterial reaction center

Veronica R. Policht[1]†, Andrew Niedringhaus[1], Rhiannon Willow[1], Philip D. Laible[2], David F. Bocian[3], Christine Kirmaier[4], Dewey Holten[4], Tomáš Mančal[5], Jennifer P. Ogilvie[1]*

We report two-dimensional electronic spectroscopy (2DES) experiments on the bacterial reaction center (BRC) from purple bacteria, revealing hidden vibronic and excitonic structure. Through analysis of the coherent dynamics of the BRC, we identify multiple quasi-resonances between pigment vibrations and excitonic energy gaps, and vibronic coherence transfer processes that are typically neglected in standard models of photosynthetic energy transfer and charge separation. We support our assignment with control experiments on bacteriochlorophyll and simulations of the coherent dynamics using a reduced excitonic model of the BRC. We find that specific vibronic coherence processes can readily reveal weak exciton transitions. While the functional relevance of such processes is unclear, they provide a spectroscopic tool that uses vibrations as a window for observing excited state structure and dynamics elsewhere in the BRC via vibronic coupling. Vibronic coherence transfer reveals the upper exciton of the "special pair" that was weakly visible in previous 2DES experiments.

INTRODUCTION

In the primary steps of photosynthesis, light-harvesting antenna structures gather solar energy and transfer it to reaction centers (RCs) for processing (*1*). Compared to the colorful array of photosynthetic antenna architectures that exist in nature, the RC structures are more widely conserved. The bacterial RC (BRC) from purple bacteria (*2*) features a pseudo-twofold symmetric hexameric core of pigments (Fig. 1A) that converts excitation energy to a stable charge-separated state. The near-unity quantum efficiency of the charge separation process is remarkable (*2*, *3*), as is the high specificity with which charge separation occurs along the "A" branch of the BRC structure (*2*, *4*). In contrast to the photosystem I and photosystem II RCs in oxygenic photosynthesis, the BRC has a strongly coupled "special pair" (SP) of bacteriochlorophyll a (BChl), yielding greater spectral separation between the absorption features in the Q_y region (Fig. 1B), making the BRC a simpler system for resolving the ultrafast processes of energy transfer and charge separation (*5*). Understanding the design principles of photosynthetic systems may open new avenues for improving artificial solar-harvesting devices and has helped motivate the development of new subfields of spectroscopy and theoretical approaches to describing the nonequilibrium photosynthetic process.

The combination of ultrafast timescales (~10s fs to ps) on which photosynthetic systems perform energy transfer and charge separation and their broad absorptions arising from multiple coupled pigments in carefully tuned dielectric environments presents considerable challenges to uncovering their structure-function relationship. Two-dimensional electronic spectroscopy (2DES) can address many of these challenges and has become a powerful tool for studying photosynthetic systems (*6*–*9*). 2DES studies of the Fenna-Matthews-Olson (FMO) complex demonstrated its ability to uncover energy transfer pathways (*6*) and revealed long-lived (~ps) coherent oscillations (*10*, *11*). Similar coherent processes have been reported in other photosynthetic systems (*8*). Ultrafast pump-probe studies of the BRC by Vos and Martin (*12*, *13*) in the early 1990s provided the first observations of coherent dynamics in photosynthetic systems. These studies proposed that the coherences arose from vibrational wave packet motion on the excited electronic state delocalized across the SP and surrounding protein matrix (*13*) and might facilitate electron transfer (*14*). The initial 2DES experiments to observe long-lived coherences in FMO (*10*) proposed superpositions of delocalized electronic excited states as the origin of the coherence with similar conclusions drawn in a two-color photon echo study of an oxidized BRC (*15*). The FMO study motivated theoretical work to assess the validity of the standard methods such as Redfield theory for describing the quantum dynamics of electronic energy transfer (*16*) and to offer alternative approaches (*17*–*19*) that could better account for coherent processes. It was later noted that the frequencies of the observed coherences matched pigment vibrational modes as well as excitonic energy gaps, raising the question about the role of vibrations in explaining both the experimental observations of coherence and the high efficiency of energy (*20*–*23*) and electron transfer (*24*). The prevalence of electronic-vibrational resonances and their possible functional relevance continues to be debated (*14*, *20*, *21*, *25*–*27*). It is now understood that vibrational degrees of freedom play a dominant role in the coherent dynamics observed in 2DES studies of photosynthetic antennas (*21*, *28*, *29*) and RCs (*25*, *26*, *30*–*33*). Theoretical and experimental work has established how electronic, vibrational, and vibronic coherence is manifest in 2DES data (*7*, *21*, *28*, *34*–*37*). In addition, there have been several reports of coherence transfer in molecular systems (*38*–*43*), although determining unambiguous spectroscopic signatures of coherence transfer remains an ongoing effort.

Here, we report coherence signatures from broadband 2DES studies of the neutral BRC as it undergoes energy transfer and charge separation and compare these signatures to those obtained from monomeric BChl (*44*) as a control for purely vibrational coherence. The coherent dynamics reveal multiple quasi-resonances between

[1]Department of Physics, University of Michigan, 450 Church St, Ann Arbor, MI 48109, USA. [2]Biosciences Division, Argonne National Laboratory, Argonne, IL 60439, USA. [3]Department of Chemistry, University of California, Riverside, CA 92521, USA. [4]Department of Chemistry, Washington University, St. Louis, MO 63130, USA. [5]Faculty of Mathematics and Physics, Charles University, Ke Karlovu 5, CZ-12116 Prague 2, Czech Republic.
*Corresponding author. Email: jogilvie@umich.edu
†Present address: Department of Physics, Politecnico di Milano, 20133 Milan, Italy.

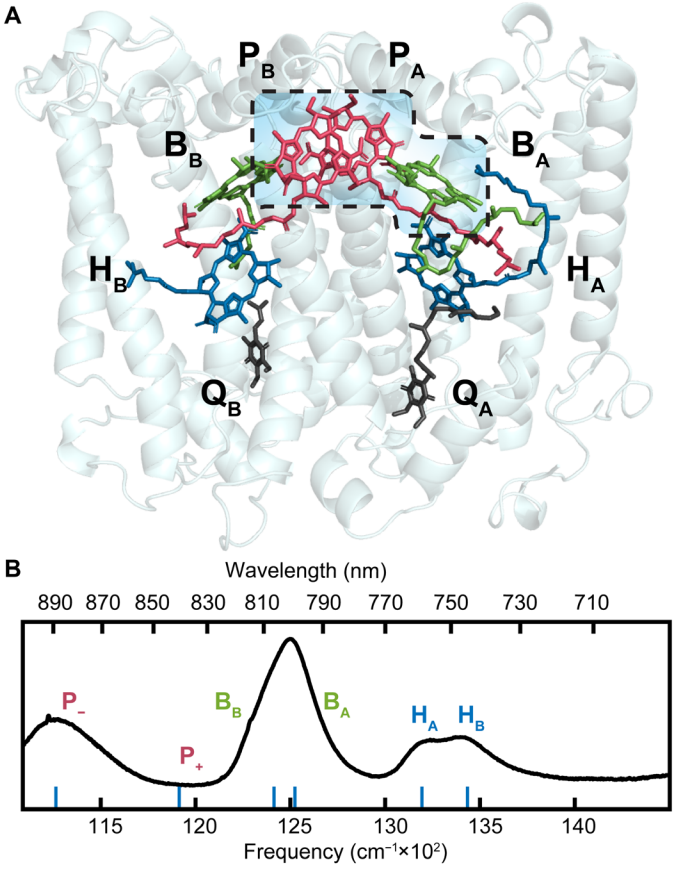

Fig. 1. Spectrum and structure of the BRC. (**A**) Structure of the BRC of *R. sphaeroides* from 2.2-Å resolution x-ray crystallography. Two BRC protein domains, L and M, are shown, with the pigments involved in energy and charge transfer highlighted and labeled for the branches active (A) and inactive (B) during charge transfer: P, special pair of BChl; B, accessory BChl; H, BPheo a; Q, quinones. *R. capsulatus* BRCs are thought to be structurally similar to the *R. sphaeroides* BRC. The W(M250)V BRC mutant studied here lacks the Q_A molecule. The figure was prepared using PyMOL with data from Protein Data Bank entry 1AIJ (*48*). (**B**) The 77 K linear absorption spectrum for the W(M250)V BRC from *R. capsulatus* is presented with excitonic peak locations, determined by Niedringhaus *et al*. (*45*), indicated by vertical blue ticks and labels.

intramolecular vibrations and electronic energy gaps identified in BRC exciton models. We find coherence signatures that cannot be explained by models of purely vibrational, electronic, or vibronic coherence. Using a reduced vibronic model of the BRC, we assign these signatures to specific vibronic coherence transfer processes. Coherence transfer processes are typically neglected in standard models of photosynthetic energy conversion, where vibrations are included in the spectral density rather than explicitly in the system Hamiltonian. We show that a subset of vibronic coherence transfer processes involves superposition states in which vibrations on the ground electronic state of one pigment provide a window for observing excited state dynamics elsewhere in the BRC via vibronic coupling. These processes can readily reveal weak exciton transitions, making vibronic coherence transfer a useful spectroscopic tool. In the case of the BRC, it allows us to confirm our recent assignment of the upper exciton transition of the SP that was only weakly visible in the 2DES correlation spectrum and required an extensive kinetic analysis for its identification (*45*). While our reduced exciton model allows us to understand the origin of the coherent signals in our data, further extensive modeling that takes into account multiple vibrational modes as well as charge transfer states will be needed to draw conclusions about the functional relevance of the observed vibronic coherence transfer processes and quasi–electronic-vibrational resonances.

Detecting coherence and coherence transfer in 2DES

In a 2DES experiment, a sequence of three laser pulses with interpulse time delays t_1 and t_2 excites the sample, inducing a third-order polarization that radiates a signal field a time t_3 after the third pulse. The amplitude and phase of this signal are recorded as a function of t_1 and t_3. A Fourier transform of the signal with respect to the t_1 and t_3 delays resolves the signal along the respective "excitation" and "detection" frequency axes of the 2D spectra at a fixed "waiting time" (t_2) (*46*). Using perturbation theory, and taking into account the experimental implementation, it is possible to enumerate all possible three-pulse interactions that contribute to the 2DES signal. These interactions can be described through so-called Liouville pathways, which chart the photo-induced time evolution of a system's density matrix represented in the basis of its eigenstates. Liouville pathways are a powerful tool for understanding the complex dynamics of a system and can be depicted using double-sided Feynman diagrams (fig. S1). A complete collection of the Liouville pathways and their associated signals would provide complete information about the time evolution of the system's photo-induced state; however, disentangling such a complete set from experimental data is usually not feasible. Here, we focus on the subset of pathways that give rise to coherent oscillatory signals during the waiting time, t_2. Such pathways originate from coherence between two eigenstates of the system, which produce beating signals at the characteristic frequency corresponding to the difference between the eigenstate energies. These beating signals can be selectively revealed by a Fourier transform with respect to the waiting time, t_2. The 2D distribution of beating signals at conjugate frequency ω_2, referred to here as a "coherence map," provides important insight into the physical origin of the coherence by enabling assignment of specific features to different Liouville pathways (*21*, *25*, *26*, *28*, *36*).

RESULTS

2DES of the BRC

We performed 2DES experiments on the W(M250)V BRC mutant of *Rhodobacter capsulatus*, which lacks the A side quinone (Fig. 1A) and performs charge separation to the $P^+H_A^-$ state (*47*). Figure 1B shows the linear absorption spectrum of the W(M250)V BRC at 77 K. Our understanding of the electronic structure of the BRC is informed by the structure as determined by x-ray crystallography (Fig. 1A), which allows us to estimate the electronic couplings and dipole moments of the individual molecules (*48*, *49*). The two nearly mirror symmetric branches of the BRC are composed of four BChl and two bacteriopheophytin a (BPheo or H) molecules, where the two closely spaced and strongly coupled BChl molecules are referred to as the SP (P). The electronic coupling between the SP pigments (P_A and P_B) is sufficiently strong that the two lowest excited states largely consist of linear combinations of excitations of P_A and P_B pigments and are denoted the upper (P_+) and lower (P_-) exciton states. Other couplings between pigment electronic transitions are relatively weak, and correspondingly, the remaining electronic eigenstates of the BRC are primarily localized on the weakly coupled

BChl (B) and H pigments. Throughout this paper, we use the term exciton to refer to any electronic eigenstate of the coupled BRC. The excitons with a predominant localization on B (H) are referred to as the B (H) state or exciton. To simulate the results of the 2DES experiments, we include vibrational states explicitly on one of the pigments. Vibrational states of the pigment do not perturb the electronic structure of the BRC substantially, and the eigenstates of the combined electronic-vibrational model, the so-called vibronic excitons, keep the same characteristic electronic structure, with the additional quantum number pertaining to the excitation of the vibrational mode.

Structure-based models of the BRC explain the three main peaks in the Q_y linear absorption spectrum (Fig. 1A) as arising in increasing energy from the lower (P_-) exciton of the SP, the combined BChl B_A and B_B pigments (B), and the bacteriopheophytins H_A and H_B (H). In contrast, the location of P_+ has been historically difficult to assign given its weak oscillator strength and proximity to the strong ~800-nm absorption of the B pigments (*49*). Several studies have developed excitonic models for the BRC from *Rhodobacter sphaeroides* (*49*–*51*) and *Rhodobacter viridis* (*49*). We previously proposed exciton energies for the *R. capsulatus* BRC studied here based on a multiexcitation 2D global analysis of 2DES data by Niedringhaus *et al.* (*45*). Those energies are largely consistent with the *R. sphaeroides* models but differ in the energy of P_+. While Niedringhaus *et al.* (*45*) noted that P_+ was evident as a weak cross-peak in the 2DES correlation spectrum (at $t_2 = 0$), a multiexcitation global analysis of the population kinetics assisted in the assignment of the P_+ state. This previous study focused on resolving the charge separation mechanism of the M(250)V BRC using hyperbolically sampled data spanning waiting times of femtoseconds to nanoseconds. In this present study, we focus on the coherent oscillatory signals as observed using even 10-fs t_2 time steps out to 3.5 ps to accurately resolve coherent oscillations with a 9.8-cm^{-1} frequency resolution up to a maximum frequency of 1680 cm^{-1}. As a control for purely vibrational coherence effects, we also present 2DES data of monomeric BChl (fig. S2) (*44*).

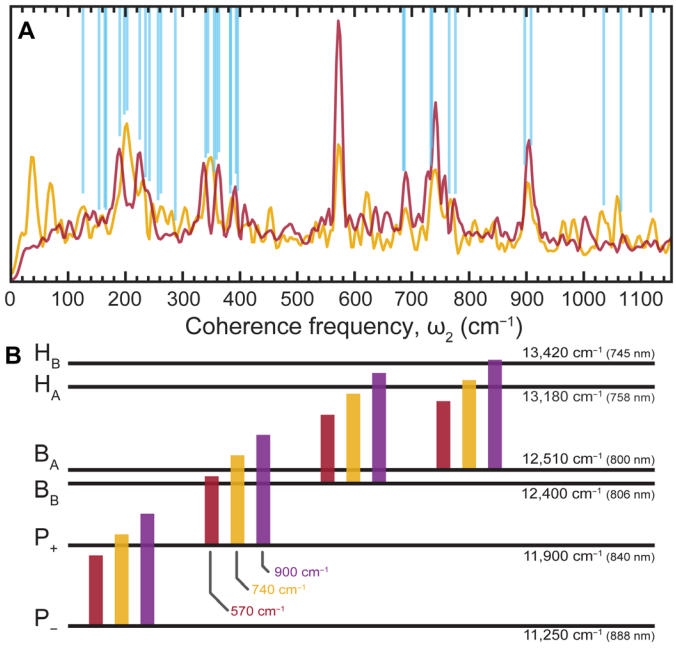

Fig. 2. Coherence frequencies observed in 2DES studies and their correspondence with the excitonic states of the BRC. (**A**) Frobenius spectra for the W(M250)V BRC (red) and bacteriochlorophyll a (gold). Blue lines indicate vibrational modes of BChl and bacteriopheophytin a (*52*–*54*) that lie within the experimental resolution (9.8 cm^{-1}) of the most prominent peaks in the Frobenius spectra. Peak prominence is determined by ≥15% of the Frobenius spectrum maximum above the background noise level. It is worth noting that the BRC Frobenius spectrum is largely dominated by B-band contributions. Several less-prominent modes not highlighted here are also in good agreement with vibrational modes such as the $\omega_2 = 656\ cm^{-1}$ mode (fig. S3). (**B**) The excitonic levels with energies taken from (*45*) demonstrate how several prominent coherence modes are in quasi-resonance with the energetic gap between excitonic levels.

Excitonic and vibronic structure in the BRC

We analyze the coherent dynamics in our 2DES data by first fitting and subtracting the population kinetics, followed by Fourier transformation of the oscillatory residual with respect to t_2. To reveal the dominant coherence frequencies that are present in the 2D spectrum during t_2, we take the "Frobenius norm," which sums over excitation (ω_{exc}) and detection frequency axes (ω_{det}) (Fig. 2A, red curve). For comparison, we also show the Frobenius spectrum of BChl in isopropanol (gold curve) (*44*). Above the Frobenius spectra, we indicate vibrational modes reported in resonance Raman experiments of BChl (*52*–*54*) and BPheo (*54*), which show good agreement with the peak positions of the Frobenius spectra. The prominent coherence modes in the Frobenius spectrum of the BRC correspond well with those reported in previous studies of coherence in the BRC (*30*–*33*) and also show good agreement with coherences reported in previous studies of BChl (*44*). The similarity between the BRC peak frequencies and the modes found in the Frobenius spectrum of monomeric BChl and the vibrational spectroscopy literature for BChl monomers (*52*–*54*) is consistent with a strong vibrational character of the BRC coherences. We note a substantial discrepancy in the low-frequency region of the Frobenius spectra, where the single peaks in the monomer spectrum at ~200 and ~340 cm^{-1} appear split into two neighboring peaks in the BRC spectrum. This splitting of the low-frequency peaks is consistent with peak frequency shifts observed in resonance Raman experiments, which selectively excited either the P_- or B bands (*52*, *55*).

Figure 2B shows the ladder of excitonic states of the BRC determined by Niedringhaus *et al.* (*45*). Superimposed on the excitonic ladder, we show the dominant coherent modes from the Frobenius spectrum of Fig. 2A, drawn with height to scale with respect to the excitonic energy gaps. It is evident from Fig. 2B that there are numerous coherent modes in quasi-resonance with excitonic energy gaps in the BRC, with an energy mismatch of tens of wavenumbers. Given that the vibrational spectra of bacteriochlorins are very dense, it is expected that there exist vibrational modes close to resonance with the excitonic energy gaps of the BRC. The interaction of electronic and vibrational degrees of freedom has been shown to lead to vibronic delocalization and modification of the allowedness of otherwise forbidden transitions (*21*–*23*, *28*).

To gain insight into the physical origin of the coherent processes in the BRC, we examine coherence maps, which display the 2D amplitude distribution at individual coherence frequencies (Fig. 3). These coherence maps are obtained by plotting, at a given ω_2, the absolute magnitude of the fast Fourier transform of the oscillatory residual (after subtraction of the population kinetics) to each (ω_{exc}, ω_{det}) point of the real rephasing 2D spectrum (*29*, *35*). By displaying the excitation and detection frequency dependence of the coherence amplitude, we can more easily assign specific peaks to particular

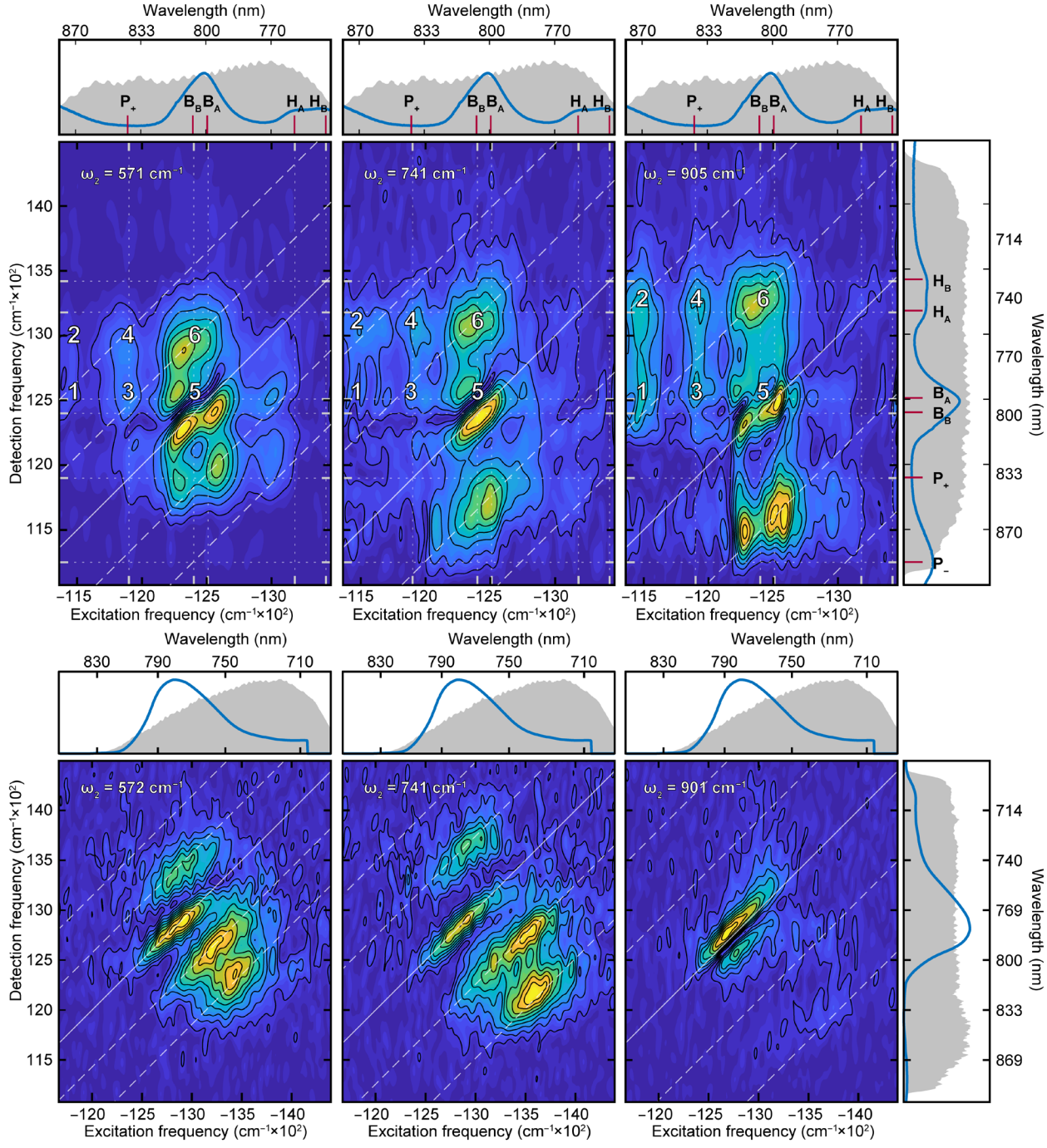

Fig. 3. Coherence amplitude maps. Coherence maps of the BRC (top row) and monomeric BChl (bottom row) reveal the distribution of the observed coherent dynamics throughout the 2D spectra. Maps are derived from the real rephasing 2D spectra at ω_2 values of 572, 741, and 905 cm^{-1} (columns left to right). For each map, the diagonal ($\omega_{exc} = \omega_{det}$) is indicated by a solid diagonal line, and parallel dashed white lines are offset from the diagonal by $\pm\omega_2$ and $\pm2\omega_2$ to aid in their interpretation. Top row: BRC excitonic energies taken from (*45*) are indicated by white dotted vertical and horizontal lines. The 77 K linear absorption spectrum, pump, and probe spectra are shown for easy reference for both BRC and BChl. Top row: Signatures labeled 1 to 6 show evidence for vibronic coupling between the P_{+}, P_{-}, and B_A states and are discussed in more detail in the text.

Liouville pathways (see figs. S7 and S8). Further details of the coherence analysis are provided in the Supplementary Materials.

Whereas the Frobenius spectra of the BRC and BChl monomer show very good agreement above ~200 cm^{-1}, clear differences between the coherence maps of the BRC and BChl monomer (Fig. 3) emerge due to the vibronic structure of the BRC. Figure 3 shows coherence maps for modes in quasi-resonance with excitonic energy gaps as identified in the Frobenius spectrum (Fig. 2A). Additional coherence maps are presented in the Supplementary Materials. The BRC coherence maps show numerous peaks, with the strongest

centered around the B transition (labeled 5 and 6). By comparing the coherence peak distribution of the signals centered around B with the BChl monomer maps (*44*) and simulated coherence maps for a simple displaced oscillator model (fig. S7), we can assign this subset of BRC peaks to a purely vibrational origin. In contrast, the peaks labeled 1 to 4 in Fig. 3 have no assignment within the simple displaced oscillator (fig. S7) (*7*, *35*, *56*), electronic dimer (*35*), or vibronic dimer models that neglect the doubly excited excitonic state (fig. S8) (*21*, *28*, *36*). Peaks labeled 1 and 2 arise at an excitation energy corresponding to the lower exciton of the SP (P_-), while peaks 3 and 4 coincide with the excitation energy of the upper exciton P_+ (*45*). A notable departure from purely vibrational coherence is the lack of diagonal peaks associated with either P_- or P_+. To understand the origin of peaks 1 to 4, we constructed a reduced vibronic model of the BRC.

Reduced vibronic model of the BRC

To assign and qualitatively describe the characteristic spectral features 1 to 4 associated with the measured coherence maps (Fig. 3), we use an effective electronic three-state model representing the two SP BChl molecules (P_A and P_B in Fig. 1A) and one accessory BChl molecule denoted as B_A. The model is reduced in the number of states with respect to the full Frenkel exciton model of the BRC to minimize the time needed to simulate 2D spectra, as both averaging over energetic disorder and exploration of a large parameter space are required. We begin with an assumption that the interesting spectral features of the ω_2 maps are a result of the vibronic interaction between electronic states and intramolecular vibrational modes of the BRC chromophores, and we put this assumption to a test in our simulations.

Our reduced vibronic model considers a single intramolecular vibrational mode (with the same frequency as experimentally observed modes) placed on either B_A or one of the SP pigments (Fig. 4A). Parameters of the model are inspired by the excitonic model of Jordanides *et al.* (*49*), from which we take the orientations of the transition dipole moments and the electronic coupling energies between the B and SP molecules (*49*). The energies of the upper and lower SP excitons are taken from (*45*) and, for simplicity, we assume that the SP is a homodimer. This allows us to fix the coupling strength between its molecules and their excitation energies by the spectral positions of the excitonic states. The parameters of our model are listed in table S2. We stress that the main aim of our simulations is not to reproduce the absorption and/or 2D spectra of the studied species, but rather to investigate the origin of the specific features 1 to 4 of the coherence maps. As a result, our reduced model of the BRC can only be expected to reproduce positions of specific features of the experimental absorption and 2D spectra (positions of the SP main peak and the position of the B peak), and it is expected to fail in reproducing amplitudes of the peaks (e.g., the B transition must have roughly half the absorption since we neglect the second B, and the H transition is missing entirely since we neglect both H pigments). Because of its weak coupling, the influence of the intramolecular vibrational mode in the absorption and 2D spectra is very small and the impact of the intramolecular vibrational modes is only revealed in the coherence maps. We study three different frequencies of the vibrational mode and two different locations of the vibrations on the BRC molecules; however, the model only includes a single intramolecular vibrational mode at a time. Correspondingly, subtle mutual influences of vibrational modes are absent from our model, and it is expected that detailed features of experimental spectra will not be reproduced quantitatively. The qualitative character of the expected agreement between the experiment and the simulation also precludes consideration of other effects that have a potential to modify the amplitudes of spectra in the region of interest, such as non-Condon effects or the presence of charge transfer states in the SP. However, the fact that vibronic effects alone seem to consistently reproduce the observed features qualitatively is a strong indication that they form a leading contribution to the experimentally observed ω_2 maps in the spectral region of interest.

Two-dimensional electronic spectra are calculated by first listing all Liouville pathways corresponding to the third-order nonlinear response of the simulated model system. We collect both rephasing and nonrephasing Liouville pathways for the ground-state bleach (GSB), stimulated emission (SE), and excited state absorption (ESA) contributions to the 2D spectrum. We ignore the so-called double coherence contributions, which arise only during pulse overlap. Instead of calculating the full 2D spectra, we preselect only those pathways that oscillate in the waiting time t_2 with the given frequency ω_2

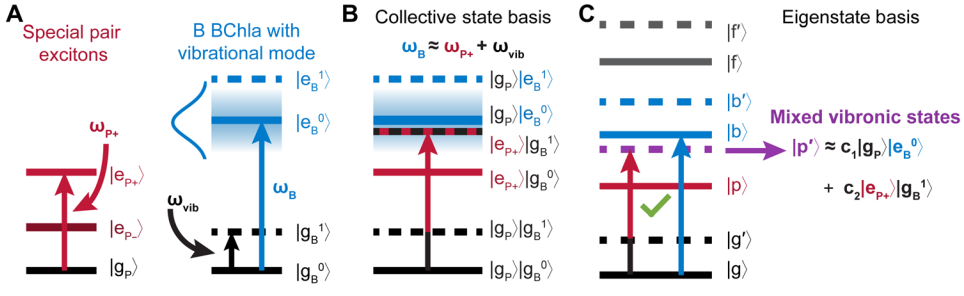

Fig. 4. Cartoon reduced excitonic model of the BRC. (**A**) Site basis representation of the reduced Frenkel exciton model where the strongly coupled special pair molecules are represented by their delocalized excitonic states ($|e_{P+}\rangle$, $|e_{P-}\rangle$) formed by electronic coupling between the special pair molecules, $J_{PP} = 325\ cm^{-1}$ (table S2). The nearest-neighbor accessory BChl ($|e_B\rangle$) additionally has one excited vibrational state on the ground ($|g_B{}^1\rangle$) and excited ($|e_B{}^1\rangle$) electronic states. The inhomogeneously broadened excited electronic state of B ($|e_B{}^0\rangle$) is represented with a Gaussian distribution of 100 cm^{-1} width (blue gradient). (**B**) The collective state basis represents the same states as in (A), demonstrating the near resonance of two key transitions: $|g_P\rangle|e_B{}^0\rangle$ and $|e_{P+}\rangle|g_B{}^1\rangle$. (**C**) The eigenstate basis includes electronic coupling, $J_{PB} = 100\ cm^{-1}$ (table S2), between the P and B sites and results in mixing between the two near-resonant transitions $|g_P\rangle|e_B{}^0\rangle$ and $|e_{P+}\rangle|g_B{}^1\rangle$. The electronic mixing enhances the allowedness of state $|p'\rangle$, which involves simultaneous excitation of the special pair excited state and the ground-state coherence of B ($|e_{P+}\rangle|g_B{}^1\rangle$). Eigenstate $|p'\rangle$ is the key state giving rise to signatures 3 and 4 and the corresponding lower exciton special pair state in signatures 1 and 2 (Fig. 3). (B) and (C) focus on the P upper exciton for visual simplicity; a more complete eigenstate diagram is presented in Fig. 6. The relative energy gaps and vibrational modes are not drawn to scale.

of the vibrational mode and thus calculate only the part of the 2D spectrum that contributes to a selected coherence map. By such a procedure, which is based on inspecting states from which the pathways are composed without evaluating their contribution to the 2D spectrum, we remove the nonoscillating part of the signal and also the part of the spectrum oscillating at other frequencies. In this way, we avoid evaluating Liouville pathways that are not expected to contribute to the final coherence map. The ignored pathways correspond to a majority of the total ensemble of pathways. We represent the simulated signals as 2D coherence maps and compare the resulting peak distributions to experiment in Fig. 5.

We find that our reduced model reproduces the characteristic BRC peaks 1 to 4 in the experimental spectra (Fig. 3) only when the vibrational mode resides on the B pigment (Fig. 4A) rather than on one of the SP pigments (fig. S24). This is unexpected, as the positions of the peaks suggest that the first excitation of the system involves P_+ or P_-, and appears unrelated to the formation of the vibrational coherence on B. To characterize the influence of resonance between the vibrational frequency and the energy gaps, we performed a parameter scan over the P_+ − B energy gap, ΔE, for the three vibrational frequencies ω = 570, 740, and 900 cm^{-1}. The results are presented in the form of movies (see table S1) with the energy gap as a running parameter. In all three cases, the experimentally observed peak pattern is reproduced in quasi-resonance conditions, when the electronic energy gap is smaller than the vibrational frequency (fig. S9). Exact resonance between the vibrational frequency and the electronic energy gap produces a pattern with peak amplitudes that are visibly inconsistent with the experimental observations.

DISCUSSION

Features 1 to 4 in the coherence maps are clearly of a mixed, i.e., vibronic origin: They appear at ω_2 frequencies that match the vibrational frequency and are absent in simulations where coupling between the SP and B_A is set to zero. From a detailed analysis of the Liouville pathways associated with each peak and the composition of the system eigenstates, we can conclude that the mixing between the electronic and vibrational states in the quasi-resonant case is rather weak. In quasi-resonance, just as in exact resonance, vibrational states can borrow oscillator strength from the electronic transitions by forming mixed vibrational-electronic (vibronic) eigenstates. It was previously found that the resonance condition for enhancement of vibrational coherence in 2DES is rather broad (*28*) and does not require an exact resonance between electronic and vibrational energy gaps. In contrast, under the quasi-resonance conditions, the observed oscillatory frequency is almost identical to the vibrational frequency of the original intramolecular mode, and the eigenstates of the BRC largely keep their original electronic character such that the resulting energy gaps between eigenstates are not substantially changed by the level repulsion. However, some previously forbidden states, notably those containing vibrational excitation in the electronic ground-state, acquire nonzero, albeit small, transition dipole moment (Fig. 4C). Crucially, the condition of quasi-resonance allows vibrational modes with a broad range of frequencies to have enhanced spectroscopic signatures. As a result, different coherence frequencies can produce similar patterns of coherence amplitude distribution in 2DES, consistent with our observations in Fig. 3A. The hallmark of the quasi-resonant case is the "stable" ω_2 frequency of the features, which always corresponds to the vibrational frequency.

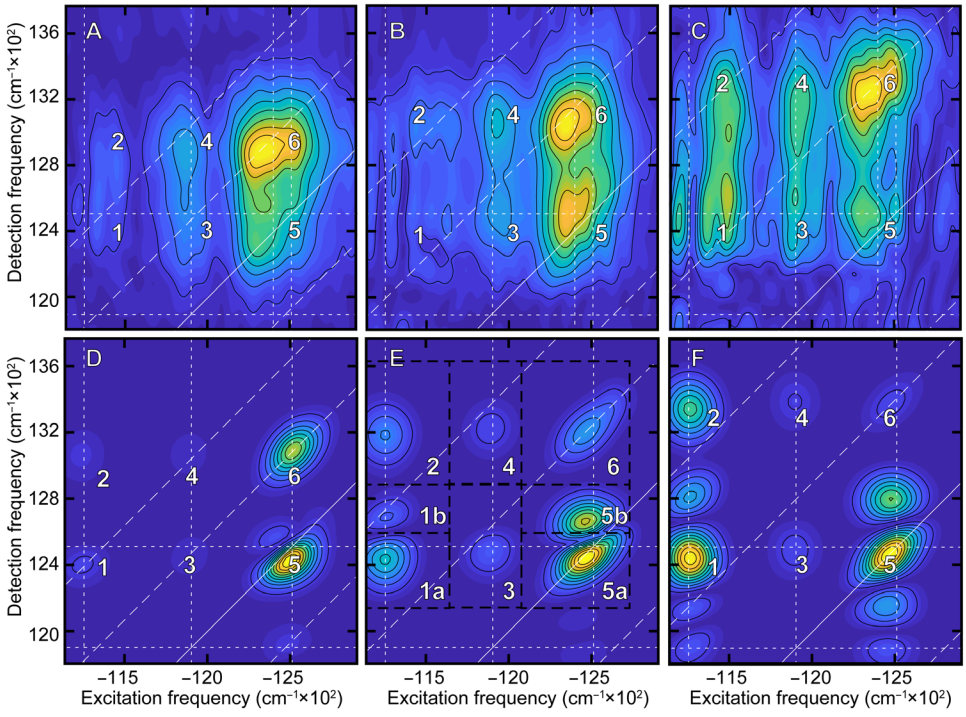

Fig. 5. Comparison of experimental and simulated positive frequency coherence maps. Experimental (**A** to **C**) and simulated (**D** to **F**) complex rephasing coherence maps for ω_2 = +570, +740, and +900 cm^{-1} featuring the prominent signatures (labeled 1 to 6) of vibronic coherence between special pair and accessory BChl sites. Prominent pathways found in regions 1 to 6 were detailed in Fig. 6.

In the resonant case, on the other hand, the frequency of the vibronic features can be shifted appreciably due to strong vibronic mixing. In addition, the condition of resonance is not simultaneously possible with all three vibrational modes observed in the experiment. Whether the effects of transition dipole moment borrowing and/or energy gap shifts can be resolved with increasing detuning from the resonance depends only on the sensitivity of the spectroscopic method. The present spectroscopic method is sufficiently sensitive to resolve very small vibronic borrowing effects on otherwise forbidden collective states, while small shifts of oscillatory frequencies are neglected (they are well within the spectral linewidths). Quasi-resonance is thus an experiment-specific condition, which (i) leverages the presence of multiple distinct intramolecular vibrational modes in pigment molecules, (ii) simplifies assignment of spectroscopic features as the optical transitions correspond well to an unperturbed excitonic model, and (iii) allows an easy verification of the condition by observing the same/similar spectroscopic features with different vibrational frequencies.

On the basis of the simulations, we are able to assign a set of Liouville pathways to each peak labeled 1 to 6 in the experimental coherence maps (Figs. 3 and 5). An extensive list of the associated Liouville pathways can be found in the Supplementary Materials. In Fig. 6, we highlight for the 740-cm^{-1} mode the four most prominent types of coherence signatures, most of which include coherence transfer. Similar distributions were observed for the 570- and 900-cm^{-1} modes. While the coherences involved in these pathways are vibronic in nature, it is instructive to consider the leading excitonic or vibrational character in each case. These are the following: type i: decaying vibrational coherence residing in the ground or excited state of the B molecule; type ii: vibrational coherence shift from the excited state of B to its ground state accompanied by electronic energy transfer from the B molecule to the P$_-$ or P$_+$ states [this process was previously identified by Paleček *et al.* (*31*) and named energy transfer–induced coherence shift (ETICS)]; type iii: electronic to vibrational coherence transfer, in which an initial electronic coherence, such as the one between purely excitonic states of the B molecule and the P$_-$ state of the SP, is transferred into a coherence characterized by a population of an excitonic state (e.g., P$_-$) with a vibrational coherence in the ground state of the B molecule (these processes can also formally be regarded as a manifestation of ETICS); type iv: ground-state vibrational coherence on B, which acts as a spectator of the excited electronic dynamics occurring elsewhere in the system. The example type iv pathway given in Fig. 6E enables identification of the P$_+$ state during energy relaxation from P$_+$ to P$_-$.

Our simulations (Fig. 5) confirm our assignment of peaks 1 and 2 to the Liouville pathways starting with the lower exciton state P$_-$ and peaks 3 and 4 to the upper exciton state P$_+$ (Fig. 3). The process of vibrational coherence decay denoted as type i is the leading contributor in terms of amplitude to peaks 1 and 2 of the calculated spectra (Fig. 6). The notable feature of this coherence is the fact that although the process occurs nominally in the collective excited state of the BRC, it involves a vibrational mode excited in the electronic ground state of the B molecule. As is well known, excitonic states involve a single molecular excitation (possibly delocalized over several molecules), while the remaining molecules of the aggregate remain unexcited. Because of resonance interaction between the molecules, some allowed excitonic states contain vibrational excitations on the electronic ground state of the participating molecules

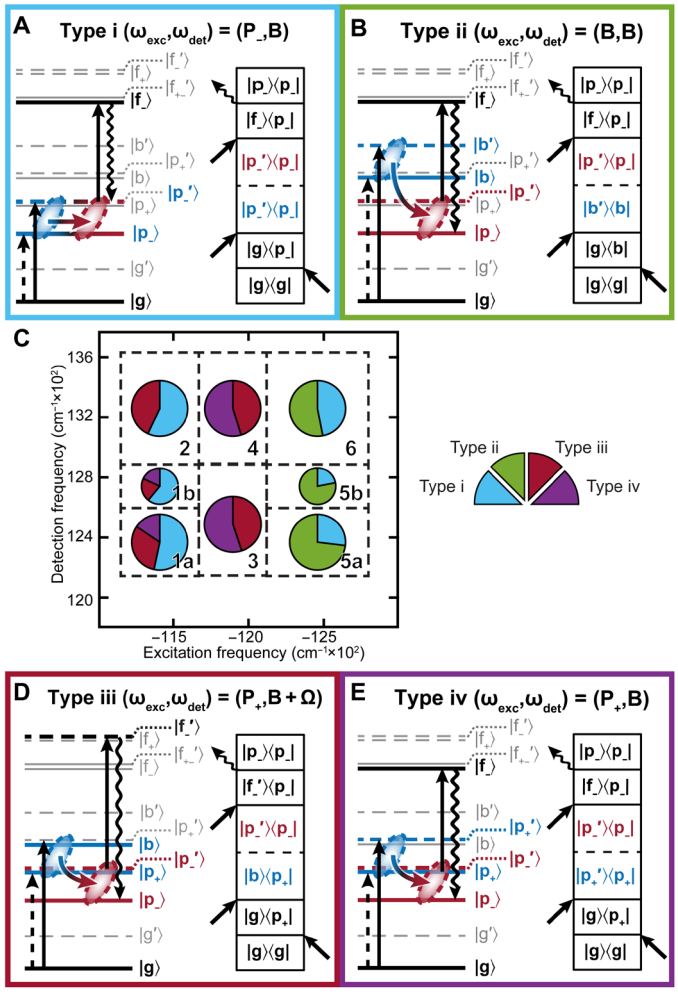

Fig. 6. Prominent coherence pathways contributing to signals in regions 1 to 6. (**A**, **B**, **D**, and **E**) Example dominant light-matter interaction pathways identified from simulations with a 740-cm^{-1} vibrational mode and represented as both light-matter Jablonski diagrams (left) and double-sided Feynman diagrams (right). (**C**) Cartoon coherence map showing the contribution of the four pathway types to each spectral region 1 to 6 at t_2 = 100 fs.

(see Fig. 4 and the Supplementary Materials for detailed information on the composition of vibronic eigenstates of the model BRC). To excite from the electronic (and vibrational) ground state of the aggregate to what is effectively a ground-state vibration, the present mechanism requires only a single interaction with the laser pulse. This makes the mechanism of vibronic enhancement at work here different from the one discussed by Tiwari *et al.* (*21*), where the observed oscillations are part of the GSB signal wherein the vibrational coherence in the electronic ground state is excited after two interactions of the field with the system. Type i coherence is more closely related to the excited state vibronic coherence described by Christensson *et al.* (*28*), with the distinction that the oscillating signal measured in the present work corresponds to ESA rather than SE.

Peaks 3 and 4 (Fig. 3) are dominated by Liouville pathways involving energy transfer from state P$_+$ to P$_-$ in a process of type iv (Fig. 6E). Here, we first excite the state P$_+$ and the vibrational coherence on

the B molecule. During t_2, population of P_+ transfers to P_-, while the vibrational coherence in the ground state of the B molecule remains largely unaffected. However, its presence allows us to observe the energy relaxation process in the coherence map. Another dominant pathway contributing to peaks 3 and 4 is a type of ETICS process (type iii), an example of which is given in Fig. 6D. A detailed account of the Liouville pathways identified in our simulations as leading contributions to signals 1 to 6 can be found in the Supplementary Materials.

We note the utility of Type iv coherence in revealing elusive states such as P_+. The P_+ state is weakly present in the real absorptive 2DES data (fig. S2A) and was assigned to an energy of 11,900 cm^{-1} after extensive kinetic analysis (*45*). In contrast, coherence analysis renders this state easy to detect (fig. S10). The assignment of P_+ is notable given the difficulty of determining the location of P_+ in previous studies of BRCs. Experimental studies of *R. sphaeroides* locate P_+ between 12,225 and 12,642 cm^{-1} (818 to 791 nm) (*51*, *57*, *58*) at 1.5 to 10 K and at 12,121 cm^{-1} (825 nm) at room temperature (*59*), while a theoretical model predicts P_+ at 12,346 cm^{-1} (810 nm) and 12,285 cm^{-1} (814 nm) at 77 K and room temperature, respectively (*49*). The site energies and couplings of the SP molecules also depend on experimental factors including temperature and solvent composition (*4*). The discrepancies between our assignment of 11,900 cm^{-1} (840 nm) to P_+ in the *R. capsulatus* BRC and BRCs in other works may also be a result of differences between bacterial species studied. The ability to reveal signatures of dark states through coherence map analysis has been reported in 2DES (*60*) and 2D infrared (IR) spectroscopy studies (*43*). Vibrational coherence transfer has been previously reported in 2D IR experiments (*42*), 2DES studies of silver nanoclusters (*41*), and transient absorption experiments probing passage through conical intersections (*40*).

Vibronic coherence transfer identified in this work must be distinguished from electronic coherence transfer processes. While coherence transfer between excitonic states can be identified in photosynthetic systems with strong coupling to environment and substantially different reorganization energies on the involved molecular transitions (*61*, *62*) and it has been proposed that coherence transfer contributions to 2DES signals can be sizeable in strongly coupled systems (*63*), most theories of photosynthetic energy transfer have focused on population transfer, ignoring coherence transfer processes and invoking the "secular approximation" (*64*). In the secular approximation, the evolution of the populations and coherences are independent of each other, and coherence transfer processes are neglected: Liouville pathways involving excited- and ground- state coherence during the time interval t_2 can only decay, and cannot drive other coherences or populations, nor can they be fed from other coherences or populations. Electronic effects beyond the secular approximation are manifested spectroscopically, e.g., by temperature-dependent absorption band shifts (*61*, *62*). At a given temperature, however, these absorption band shifts can be understood as an effective localization of the system's excitonic states due to strong interaction with environment (i.e., as an effective reduction of coupling between involved molecular states). The electronic part of the system can thus be represented by an effective Hamiltonian accounting for energy and coupling renormalization. To this Hamiltonian, a theory of electronic energy transfer in the secular approximation is applied. The vibronic states assigned in this work then represent superpositions of localized vibrational states and the states of the effective electronic Hamiltonian.

The spectroscopic signatures we observe in the BRC suggest the possible importance of electronic-vibrational resonances and coherence transfer processes involving vibrations on B. There is ongoing discussion in the literature regarding the possible functional role of specific vibrations in assisting the transfer of electronic excitation energy (*20*, *21*, *65*–*67*), with some studies suggesting no enhancement effect, or only weakly enhanced energy transfer (*68*–*70*). Such a role for electronic-vibrational resonances has been proposed in other photosynthetic systems (*20*, *21*), as has their possible importance for downhill energy transfer from H to B in the BRC (*31*). Recent 2DES studies of BRCs have reported that particular low-frequency quasi-resonances (<200 cm^{-1}) between exciton and charge-transfer states are correlated with high charge separation efficiency (*30*, *33*). However, the functional relevance of these quasi-resonances for charge separation remains a topic of debate (*14*, *27*).

In conclusion, we report previously hidden excitonic and vibronic structure in the BRC, revealed through analysis of coherent 2DES signals. We confirm the assignment of the elusive SP upper exciton state and find numerous quasi–electronic-vibrational resonances in the BRC. Through a comparison of the monomer BChl and BRC 2DES coherence maps along with simulations of a reduced BRC model, we identify vibronic coherence transfer processes involving the SP and B pigments, in which vibrations on B play a prominent role. The possible functional importance of such processes, as well as quasi–electronic-vibrational resonances to photosynthetic energy transfer and charge separation, merits further theoretical and experimental examination.

MATERIALS AND METHODS

2DES measurements

All experimental data presented here were collected using a hybrid diffractive optic and pulse shaping based 2DES setup, which uses an acousto-optic programmable dispersive filter (AOPDF) pulse shaper (Dazzler, Fastlite) to simultaneously collect rephasing, nonrephasing, and transient grating signals (*71*). Interpulse delay between the first and second pump pulses was scanned $0 < t_1 < 390$ fs in 10-fs steps; the waiting time between the second pump and the probe, t_2, was scanned in 10-fs steps from $-50 < t_2 < 3500$ fs. Data were truncated at $80 < t_2 < 3500$ fs before coherence analysis to eliminate contributions from coherent transients, resulting in a coherence frequency resolution of 9.8 cm^{-1} and maximum resolvable coherence frequency of 1668 cm^{-1}. Light pulses were generated using a homebuilt optical parametric amplifier (OPA) pumped and seeded by a 500-Hz, 40-fs, Ti:sapphire regenerative amplifier regen (Spitfire XP, Spectra-Physics) centered at 800 nm. Both experiments used pumps, probe, and local oscillator from the same degenerate OPA (DOPA) (*72*) (spectra shown in fig. S2). The pump used in the BRC (BChl) experiment was compressed to 14.5 (14.3) fs with an AOPDF and the probe to 10.3 (10) fs using chirped mirrors and an SLM (spatial light modulator) pulse shaper (femtoJock, BioPhotonic Solutions).

All experiments shown here were conducted at 77 K in a LN_2 cryostat (Microstat, Oxford Instruments) with a 380-μm path length cell. Samples were prepared to have an average optical density (OD) ≈ 0.3, although the BRCs were prepared with higher peak OD to better resolve the lower dipole-strength SP. BChl samples were prepared from powder purchased from Sigma-Aldrich and were dissolved in isopropanol, which was degassed using N_2 gas before sample preparation. The sample was handled and loaded under N_2 atmosphere in a glove box.

Sample preparation

W(M250)V BRC mutants were isolated and kept in pH 7.8 10 mM tris with 0.1% Deriphat buffer. Before concentration, BRC samples were treated with 40 mM terbutryn to remove or inactivate quinones and 400 mM sodium ascorbate to reduce the SP between laser shots. Following concentration, BRCs in buffer were mixed with glycerol (1:1, v/v) to ensure good quality glass when frozen.

SUPPLEMENTARY MATERIALS

Supplementary material for this article is available at https://science.org/doi/10.1126/sciadv.abk0953

REFERENCES AND NOTES

1. R. E. Blankenship, *Molecular Mechanisms of Photosynthesis* (Blackwell Science Ltd, 2008).
2. W. W. Parson, A. Warshel, Mechanism of charge separation in purple bacterial reaction centers, in *The Purple Phototrophic Bacteria*, vol. 28 of *Advances in Photosynthesis and Respiration*, C. N. Hunter, F. Daldal, M. C. Thurnauer, J. T. Beatty, Eds. (Springer, 2009), pp. 355–377.
3. C. A. Wraight, R. K. Clayton, The absolute quantum efficiency of bacteriochlorophyll photooxidation in reaction centres of *Rhodopseudomonas spheroides*. *Biochim. Biophys. Acta Bioenerg.* **333**, 246–260 (1974).
4. C. Kirmaier, D. Holten, W. W. Parson, Picosecond-photodichroism studies of the transient states in *Rhodopseudomonas sphaeroides* reaction centers at 5 K. Effects of electron transfer on the six bacteriochlorin pigments. *Biochim. Biophys. Acta Bioenerg.* **810**, 49–61 (1985).
5. L. M. Yoder, A. G. Cole, R. J. Sension, Structure and function in the isolated reaction center complex of photosystem II: Energy and charge transfer dynamics and mechanism. *Photosynth. Res.* **72**, 147–158 (2002).
6. T. Brixner, J. Stenger, H. M. Vaswani, M. Cho, R. E. Blankenship, G. R. Fleming, Two-dimensional spectroscopy of electronic couplings in photosynthesis. *Nature* **434**, 625–628 (2005).
7. D. B. Turner, R. Dinshaw, K.-K. Lee, M. S. Belsley, K. E. Wilk, P. M. G. Curmi, G. D. Scholes, Quantitative investigations of quantum coherence for a light-harvesting protein at conditions simulating photosynthesis. *Phys. Chem. Chem. Phys.* **14**, 4857–4874 (2012).
8. G. D. Scholes, G. R. Fleming, A. Olaya-Castro, R. Van Grondelle, Lessons from nature about solar light harvesting. *Nat. Chem.* **3**, 763–774 (2011).
9. K. L. M. Lewis, J. P. Ogilvie, Probing photosynthetic energy and charge transfer with two-dimensional electronic spectroscopy. *J. Phys. Chem. Lett.* **3**, 503–510 (2012).
10. G. S. Engel, T. R. Calhoun, E. L. Read, T.-K. Ahn, T. Mančal, Y.-C. Cheng, R. E. Blankenship, G. R. Fleming, Evidence for wavelike energy transfer through quantum coherence in photosynthetic systems. *Nature* **446**, 782–786 (2007).
11. G. Panitchayangkoon, D. Hayes, K. A. Fransted, J. R. Caram, E. Harel, J. Wen, R. E. Blankenship, G. S. Engel, Long-lived quantum coherence in photosynthetic complexes at physiological temperature. *Proc. Natl. Acad. Sci. U.S.A.* **107**, 12766–12770 (2010).
12. M. H. Vos, J. C. Lambry, S. J. Robles, D. C. Youvan, J. Breton, J. L. Martin, Direct observation of vibrational coherence in bacterial reaction centers using femtosecond absorption spectroscopy. *Proc. Natl. Acad. Sci. U.S.A.* **88**, 8885–8889 (1991).
13. M. H. Vos, J. L. Martin, Femtosecond processes in proteins. *Biochim. Biophys. Acta* **1411**, 1–20 (1999).
14. E. Romero, V. I. Novoderezhkin, R. Van Grondelle, Quantum design of photosynthesis for bio-inspired solar-energy conversion. *Nature* **543**, 355–365 (2017).
15. H. Lee, Y.-C. Cheng, G. R. Fleming, Coherence dynamics in photosynthesis: Protein protection of excitonic coherence. *Science* **316**, 1462–1465 (2007).
16. A. Ishizaki, G. R. Fleming, On the adequacy of the Redfield equation and related approaches to the study of quantum dynamics in electronic energy transfer. *J. Chem. Phys.* **130**, 234110 (2009).
17. A. Ishizaki, G. R. Fleming, Unified treatment of quantum coherent and incoherent hopping dynamics in electronic energy transfer: Reduced hierarchy equation approach. *J. Chem. Phys.* **130**, 234111 (2009).
18. A. W. Chin, Á. Rivas, S. F. Huelga, M. B. Plenio, Exact mapping between system-reservoir quantum models and semi-infinite discrete chains using orthogonal polynomials. *J. Math. Phys.* **51**, 092109 (2010).
19. P. Huo, D. F. Coker, Iterative linearized density matrix propagation for modeling coherent excitation energy transfer in photosynthetic light harvesting. *J. Chem. Phys.* **133**, 184108 (2010).
20. J. M. Womick, A. M. Moran, Vibronic enhancement of exciton sizes and energy transport in photosynthetic complexes. *J. Phys. Chem. B* **115**, 1347–1356 (2011).
21. V. Tiwari, W. K. Peters, D. M. Jonas, Electronic resonance with anticorrelated pigment vibrations drives photosynthetic energy transfer outside the adiabatic framework. *Proc. Natl. Acad. Sci. U.S.A.* **110**, 1203–1208 (2013).
22. A. Kolli, E. J. O'Reilly, G. D. Scholes, A. Olaya-Castro, The fundamental role of quantized vibrations in coherent light harvesting by cryptophyte algae. *J. Chem. Phys.* **137**, 174109 (2012).
23. S. F. Huelga, M. B. Plenio, Vibrations, quanta and biology. *Contemp. Phys.* **54**, 181–207 (2013).
24. N. Renaud, D. Powell, M. Zarea, B. Movaghar, M. R. Wasielewski, M. A. Ratner, Quantum interferences and electron transfer in photosystem I. *J. Phys. Chem. A* **117**, 5899–5908 (2013).
25. F. D. Fuller, J. Pan, A. Gelzinis, V. Butkus, S. S. Senlik, D. E. Wilcox, C. F. Yocum, L. Valkunas, D. Abramavicius, J. P. Ogilvie, Vibronic coherence in oxygenic photosynthesis. *Nat. Chem.* **6**, 706–711 (2014).
26. E. Romero, R. Augulis, V. I. Novoderezhkin, M. Ferretti, J. Thieme, D. Zigmantas, R. Van Grondelle, Quantum coherence in photosynthesis for efficient solar-energy conversion. *Nat. Phys.* **10**, 676–682 (2014).
27. Y. Fujihashi, M. Higashi, A. Ishizaki, Intramolecular vibrations complement the robustness of primary charge separation in a dimer model of the photosystem II reaction center. *J. Phys. Chem. Lett.* **9**, 4921–4929 (2018).
28. N. Christensson, H. F. Kauffmann, T. Pullerits, T. Mančal, Origin of long-lived coherences in light-harvesting complexes. *J. Phys. Chem. B* **116**, 7449–7454 (2012).
29. J. Cao, R. J. Cogdell, D. F. Coker, H.-G. Duan, J. Hauer, U. Kleinekathöfer, T. L. C. Jansen, T. Mančal, R. J. D. Miller, J. P. Ogilvie, V. I. Prokhorenko, T. Renger, H.-S. Tan, R. Tempelaar, M. Thorwart, E. Thyrhaug, S. Westenhoff, D. Zigmantas, Quantum biology revisited. *Sci. Adv.* **6**, eaaz4888 (2020).
30. S. Westenhoff, D. Paleček, P. Edlund, P. Smith, D. Zigmantas, Coherent picosecond exciton dynamics in a photosynthetic reaction center. *J. Am. Chem. Soc.* **134**, 16484–16487 (2012).
31. D. Paleček, P. Edlund, S. Westenhoff, D. Zigmantas, Quantum coherence as a witness of vibronically hot energy transfer in bacterial reaction center. *Sci. Adv.* **3**, e1603141 (2017).
32. M. L. Flanagan, P. D. Long, P. D. Dahlberg, B. S. Rolczynski, S. C. Massey, G. S. Engel, Mutations to *R. sphaeroides* reaction center perturb energy levels and vibronic coupling but not observed energy transfer rates. *J. Phys. Chem. A* **120**, 1479–1487 (2016).
33. I. S. Ryu, H. Dong, G. R. Fleming, Role of electronic-vibrational mixing in enhancing vibrational coherences in the ground electronic states of photosynthetic bacterial reaction center. *J. Phys. Chem. B* **118**, 1381–1388 (2014).
34. A. Chenu, N. Christensson, H. F. Kauffmann, T. Mančal, Enhancement of Vibronic and ground-state vibrational coherences in 2D spectra of photosynthetic complexes. *Sci. Rep.* **3**, 2029 (2013).
35. V. Butkus, D. Zigmantas, D. Abramavicius, L. Valkunas, Distinctive character of electronic and vibrational coherences in disordered molecular aggregates. *Chem. Phys. Lett.* **587**, 93–98 (2013).
36. V. Butkus, L. Valkunas, D. Abramavicius, Vibronic phenomena and exciton–vibrational interference in two-dimensional spectra of molecular aggregates. *J. Chem. Phys.* **140**, 034306 (2014).
37. A. Halpin, P. J. M. Johnson, R. Tempelaar, R. S. Murphy, J. Knoester, T. L. C. Jansen, R. J. D. Miller, Two-dimensional spectroscopy of a molecular dimer unveils the effects of vibronic coupling on exciton coherences. *Nat. Chem.* **6**, 196–201 (2014).
38. D. A. Farrow, W. Qian, E. R. Smith, A. A. Ferro, D. M. Jonas, Polarized pump-probe measurements of electronic motion via a conical intersection. *J. Chem. Phys.* **128**, 144510 (2008).
39. J. Brazard, L. A. Bizimana, T. Gellen, W. P. Carbery, D. B. Turner, Experimental detection of branching at a conical intersection in a highly fluorescent molecule. *J. Phys. Chem. Lett.* **7**, 14–19 (2016).
40. A. J. Musser, M. Liebel, C. Schnedermann, T. Wende, T. B. Kehoe, A. Rao, P. Kukura, Evidence for conical intersection dynamics mediating ultrafast singlet exciton fission. *Nat. Phys.* **11**, 352–357 (2015).
41. E. Thyrhaug, S. A. Bogh, M. R. Carro-Temboury, C. S. Madsen, T. Vosch, D. Zigmantas, Ultrafast coherence transfer in DNA-templated silver nanoclusters. *Nat. Commun.* **8**, 15577 (2017).
42. J. D. Gaynor, J. Sandwisch, M. Khalil, Vibronic coherence evolution in multidimensional ultrafast photochemical processes. *Nat. Commun.* **10**, 5621 (2019).
43. P. A. Eckert, K. J. Kubarych, Vibrational coherence transfer illuminates dark modes in models of the FeFe hydrogenase active site. *J. Chem. Phys.* **151**, 054307 (2019).
44. V. R. Policht, A. Niedringhaus, J. P. Ogilvie, Characterization of vibrational coherence in monomeric bacteriochlorophyll a by two-dimensional electronic spectroscopy. *J. Phys. Chem. Lett.* **9**, 6631–6637 (2018).
45. A. Niedringhaus, V. R. Policht, R. Sechrist, A. Konar, P. D. Laible, D. F. Bocian, D. Holten, C. Kirmaier, J. P. Ogilvie, Primary processes in the bacterial reaction center probed by two-dimensional electronic spectroscopy. *Proc. Natl. Acad. Sci. U.S.A.* **115**, 3563–3568 (2018).

46. D. M. Jonas, Two-dimensional femtosecond spectroscopy. *Annu. Rev. Phys. Chem.* **54**, 425–463 (2003).
47. K. M. Faries, N. P. Dylla, D. K. Hanson, D. Holten, P. D. Laible, C. Kirmaier, Manipulating the energetics and rates of electron transfer in *Rhodobacter capsulatus* reaction centers with asymmetric pigment content. *J. Phys. Chem. B* **121**, 6989–7004 (2017).
48. M. H. B. Stowell, T. M. McPhillips, D. C. Rees, S. M. Soltis, E. Abresch, G. Feher, Light-induced structural changes in photosynthetic reaction center: Implications for mechanism of electron-proton transfer. *Science* **276**, 812–816 (1997).
49. X. J. Jordanides, G. D. Scholes, G. R. Fleming, The mechanism of energy transfer in the bacterial photosynthetic reaction center. *J. Phys. Chem. B* **105**, 1652–1669 (2001).
50. O. Rancova, R. Jankowiak, A. Kell, M. Jassas, D. Abramavicius, Band structure of the *Rhodobacter sphaeroides* photosynthetic reaction center from low-temperature absorption and hole-burned spectra. *J. Phys. Chem. B* **120**, 5601–5616 (2016).
51. J. Breton, A. Vermeglio, *The Photosynthetic Bacterial Reaction Center* (Springer US, 1988), vol. 149.
52. K. Czarnecki, J. R. Diers, V. Chynwat, J. P. Erickson, H. A. Frank, D. F. Bocian, Characterization of the strongly coupled, low-frequency vibrational modes of the special pair of photosynthetic reaction centers via isotopic labeling of the cofactors. *J. Am. Chem. Soc.* **119**, 415–426 (1997).
53. J. R. Diers, D. F. Bocian, Qy-excitation resonance Raman spectra of bacteriochlorophyll observed under fluorescence-free conditions. Implications for cofactor structure in photosynthetic proteins. *J. Am. Chem. Soc.* **117**, 6629–6630 (1995).
54. M. Lutz, J. Kleo, F. Reiss-Husson, Resonance Raman scattering of bacteriochlorophyll, bacteriopheophytin and spheroidene in reaction centers of Rhodopseudomonas spheroides. *Biochem. Biophys. Res. Commun.* **69**, 711–717 (1976).
55. V. Palaniappan, C. C. Schenck, D. F. Bocian, Low-frequency near-infrared-excitation resonance Raman spectra of (M)H202L mutant reaction centers from rhodobacter sphaeroides. implications for the structural, vibronic, and electronic properties of the bacteriochlorin cofactors. *J. Phys. Chem.* **99**, 17049–17058 (1995).
56. D. Egorova, Detection of electronic and vibrational coherences in molecular systems by 2D electronic photon echo spectroscopy. *Chem. Phys.* **347**, 166–176 (2008).
57. S. R. Meech, A. J. Hoff, D. A. Wiersma, Role of charge-transfer states in bacterial photosynthesis. *Proc. Natl. Acad. Sci. U.S.A.* **83**, 9464–9468 (1986).
58. G. Hartwich, H. Scheer, V. Aust, A. Angerhofer, Absorption and ADMR studies on bacterial photosynthetic reaction centres with modified pigments. *Biochim. Biophys. Acta* **1230**, 97–113 (1995).
59. D. C. Arnett, C. C. Moser, P. L. Dutton, N. F. Scherer, The first events in photosynthesis: Electronic coupling and energy transfer dynamics in the photosynthetic reaction center from *Rhodobacter sphaeroides*. *J. Phys. Chem. B* **103**, 2014–2032 (1999).
60. A. A. Bakulin, S. E. Morgan, T. B. Kehoe, M. W. B. Wilson, A. W. Chin, D. Zigmantas, D. Egorova, A. Rao, Real-time observation of multiexcitonic states in ultrafast singlet fission using coherent 2D electronic spectroscopy. *Nat. Chem.* **8**, 16–23 (2016).
61. T. Renger, Theory of optical spectra involving charge transfer states: Dynamic localization predicts a temperature dependent optical band shift. *Phys. Rev. Lett.* **93**, 188101 (2004).
62. T. Mančal, L. Valkunas, G. R. Fleming, Theory of exciton–charge transfer state coupled systems. *Chem. Phys. Lett.* **432**, 301–305 (2006).
63. K. Hyeon-Deuk, Y. Tanimura, M. Cho, Ultrafast exciton-exciton coherent transfer in molecular aggregates and its application to light-harvesting systems. *J. Chem. Phys.* **127**, 075101 (2007).
64. V. May, O. Kuhn, *Charge and Energy Transfer Dynamics in Molecular Systems* (Wiley, 2003).
65. V. Perlík, J. Seibt, L. J. Cranston, R. J. Cogdell, C. N. Lincoln, J. Savolainen, F. Šanda, T. Mančal, J. Hauer, Vibronic coupling explains the ultrafast carotenoid-to-bacteriochlorophyll energy transfer in natural and artificial light harvesters. *J. Chem. Phys.* **142**, 212434 (2015).
66. P. Malý, O. J. G. Somsen, V. I. Novoderezhkin, T. Mančal, R. van Grondelle, The role of resonant vibrations in electronic energy transfer. *ChemPhysChem* **17**, 1356–1368 (2016).
67. P. Malý, V. I. Novoderezhkin, R. van Grondelle, T. Mančal, Electron-vibrational coupling decreases trapping by low-energy states in photosynthesis. *Chem. Phys.* **522**, 69–76 (2019).
68. C. Kreisbeck, T. Kramer, A. Aspuru-Guzik, Scalable high-performance algorithm for the simulation of exciton dynamics. Application to the light-harvesting complex II in the presence of resonant vibrational modes. *J. Chem. Theory Comput.* **10**, 4045–4054 (2014).
69. Y. Fujihashi, G. R. Fleming, A. Ishizaki, Impact of environmentally induced fluctuations on quantum mechanically mixed electronic and vibrational pigment states in photosynthetic energy transfer and 2D electronic spectra. *J. Chem. Phys.* **142**, 212403 (2015).
70. A. Ishizaki, G. R. Fleming, Insights into photosynthetic energy transfer gained from free-energy structure: Coherent transport, incoherent hopping, and vibrational assistance revisited. *J. Phys. Chem. B* **125**, 3286–3295 (2021).
71. F. D. Fuller, D. E. Wilcox, J. P. Ogilvie, Pulse shaping based two-dimensional electronic spectroscopy in a background free geometry. *Opt. Express* **22**, 1018 (2014).
72. A. M. Siddiqui, G. Cirmi, D. Brida, F. X. Kärtner, G. Cerullo, Generation of <7 fs pulses at 800 nm from a blue-pumped optical parametric amplifier at degeneracy. *Opt. Lett.* **34**, 3592–3594 (2009).
73. J. R. Diers, Y. Zhu, R. E. Blankenship, D. F. Bocian, Q_y-excitation resonance Raman spectra of chlorophyll *a* and bacteriochlorophyll *c/d* aggregates. Effects of peripheral substituents on the low-frequency vibrational characteristics. *J. Phys. Chem.* **100**, 8573–8579 (1996).
74. J. Seibt, T. Pullerits, Beating signals in 2D spectroscopy: Electronic or nuclear coherences? application to a quantum dot model system. *J. Phys. Chem. C* **117**, 18728–18737 (2013).
75. Y. Song, C. Hellmann, N. Stingelin, G. D. Scholes, The separation of vibrational coherence from ground- and excited-electronic states in P3HT film. *J. Chem. Phys.* **142**, 212410 (2015).
76. V. Butkus, D. Zigmantas, L. Valkunas, D. Abramavicius, Vibrational vs. electronic coherences in 2D spectrum of molecular systems. *Chem. Phys. Lett.* **545**, 40–43 (2012).
77. S. S. Senlik, V. R. Policht, J. P. Ogilvie, Two-color nonlinear spectroscopy for the rapid acquisition of coherent dynamics. *J. Phys. Chem. Lett.* **6**, 2413–2420 (2015).
78. G. Lindblad, Completely positive maps and entropy inequalities. *Commun. Math. Phys.* **40**, 147–151 (1975).
79. B. Fain, *Irreversibilities in Quantum Mechanics* (Springer, 2002).
80. S. Mukamel, *Principles of Nonlinear Optical Spectroscopy* (Oxford Univ. Press, 1999).
81. T. Mančal, A decade with quantum coherence : How our past became classical and the future turned quantum. *Chem. Phys.* **532**, 110663 (2020).
82. J. Olšina, T. Kramer, C. Kreisbeck, T. Mančal, Exact stochastic unraveling of an optical coherence dynamics by cumulant expansion. *J. Chem. Phys.* **141**, 164109 (2014).
83. T. Mančal, J. Dostál, J. Pšenčík, D. Zigmantas, Transfer of vibrational coherence through incoherent energy transfer process in Förster limit. *Can. J. Chem.* **92**, 135–143 (2014).

Acknowledgments

Funding: This work was funded by the NSF (grant PHY-0748470 to V.R.P., A.N., and J.P.O. and grant PHY-1607570 to V.R.P., A.N., and J.P.O.), Office of Basic Energy Sciences, U.S. Department of Energy (grant DE-SC0016384 to R.W. and J.P.O. and grant DE-CD0002036 to C.K. and D.H.), U.S. Department of Energy, Office of Basic Energy Sciences under Field Work Proposal (DE-CD0002036 to P.D.L.), Charles University Research Center Program (UNCE/SCI/010 to T.M.), and Czech Science Foundation (GAČR) (grant 18-18022S to T.M.). **Author contributions:** Conceptualization: V.R.P., A.N., and J.P.O. Methodology: J.P.O. and T.M. Investigation: V.R.P., A.N., J.P.O., R.W., C.K., D.H., and D.F.B. Resources: P.D.L., C.K., D.H., J.P.O., and T.M. Writing—original draft: V.R.P., J.P.O., and T.M. **Competing interests:** The authors declare that they have no competing interests. **Data and materials availability:** All data needed to evaluate the conclusions in the paper are present in the paper and/or the Supplementary Materials. The spectroscopic package used for theoretical simulations and the specific scripts used to generate the results presented in this paper are available at dx.doi.org/10.5281/zenodo.5513670 and dx.doi.org/10.5281/zenodo.5500157, respectively.

Submitted 22 June 2021
Accepted 11 November 2021
Published 5 January 2022
10.1126/sciadv.abk0953